Selective extraction of entangled textures via adaptive PDE transform

Yang Wang [1], Guo Wei Wei[1,2] and Siyang Yang[1]

[1]Department of Mathematics

Michigan State University, MI 48824, USA

[2]Department of Electrical and Computer Engineering

Michigan State University, MI 48824, USA

November 3, 2011

Abstract

Texture and feature extraction is an important research area with a wide range of applications in science and technology. Selective extraction of entangled textures is a challenging task due to spatial entanglement, orientation mixing and high frequency overlapping. The partial differential equation (PDE) transform is an efficient method for functional mode decomposition. The present work introduces adaptive PDE transform algorithm to appropriately threshold the statistical variance of the local variation of functional modes. The proposed adaptive PDE transform is applied to the selective extraction of entangled textures. Successful separations of human face, clothes, background, natural landscape, text, forest, camouflaged sniper and neuron skeletons have validated the proposed method.

Key words: Entangled textures; selective extraction; adaptive PDE transform; statistical analysis; neuron image.

I Introduction

Texture is one of the important features characterizing many natural and man-made images. Texture characterization and analysis are usually performed according to the spatial as well as frequency variations of brightness, pixel intensities, color and texture orientation in the different regions of the image corresponding to different types of textures. For example, the roughness or bumpiness of an image usually refers to variations in the intensity values, or gray levels. Texture segmentation, recognition

and interpretation are critical for human visual perception and processing. As a result, research on texture analysis has received considerable attention in recent years. A large number of approaches has been proposed for texture classification and segmentation.[1–8,14,17,33,42–46] In general, texture analysis methods fall into two categories: statistical methods which analyzes the Fourier power spectrum, gray level values, and various variance matrices of the input image, and structural methods which are knowledge-based algorithms with an emphasis on the structural primitives and their placement rules. Some examples of such methods include Markov random field models,[12,13] simultaneous autoregressive model,[11] and fractal models.[15] Among many existing approaches, local variation minimization has been a popular and powerful technique in image analysis[16] with applications to the texture modeling.[18] Multiphase segmentation approaches are based on the structural division of gray scales.[19] More recently, multiresolution approaches have become more important in texture analysis,[9–11,20] where fixed-size neighborhood and window size are used to derive features at varying scales corresponding to the input image at different resolutions.

In general, the total texture extraction has become a mature technique in real applications. However, despite of the progress in the past few decades, selective extraction of entangled textures encounters a number of difficulties. One difficulty is due to *spatial entanglement*, including orientation mixing of various textures. Another difficulty is due to *gray scale entanglement*, especially the near continuous merging of various textures. The other difficulty is due to *frequency entanglement* when two similar but different textures share overlapping frequency band in the frequency domain. This difficulty would especially plague texture analysis when many high frequency textures coexist.

In this work, we propose an adaptive partial differential equation (PDE) transform approach for selective extraction of entangled textures. By using arbitrarily high order PDEs, the PDE transform is able to decompose signals, images and data into functional modes, which exhibit appropriate time-frequency localizations.[21–25] Additionally, the PDE transform is able to provide a perfect reconstruction. Unlike wavelet transform or Fourier transform, the PDE transform offers results in the physical domain, which enables straightforward mode analysis and secondary processing. Based on the image mode function generated by the PDE transform method, the adaptive PDE transform algorithm calculates the variance of the local variation of the image mode functions followed by the corresponding thresholding analysis.

II PDE transform method

In the past two decades, PDE based image processing approaches have raised a strong interest in the image processing and applied mathematical communities and have opened new approaches for image

denoising, enhancement, edge detection, restoration, segmentation, etc. The use of PDEs for image analysis started as early as 1980's when Witkin first introduced diffusion equation for image denoising.[26] The time evolution of an image under a diffusion operator is formally equivalent to the low-pass filter. After Perona and Malik introduced anisotropic diffusion equation in 1990,[27] non-linear PDE has found great applications for a variety of image processing tasks such as edge detection and denoising. Two important advances in the history of image processing, namely the Perona-Malik equation and the total variation methods,[16] employ second order nonlinear PDEs for image analysis. The Willmore flow, proposed in 1920s, is a fourth order geometric PDE and has also been used for surface analysis. In the past decade, fourth order nonlinear PDEs have attracted much attention in image analysis.[28–30]

Arbitrarily high order nonlinear PDEs were introduced by Wei in 1999 to more efficiently remove image noise in edge-preserving image restoration[28]

$$u_t(\mathbf{r},t) = \sum_q \nabla \cdot \left[d_q(u,|\nabla u|) \nabla \nabla^{2q} u \right] + e(u,|\nabla u|), \quad (q = 0, 1, \cdots) \tag{1}$$

where $u \equiv u(\mathbf{r},t)$ is the image function, $d_q(u(\mathbf{r}),|\nabla u(\mathbf{r})|,t)$ and $e(u(\mathbf{r}),|\nabla u(\mathbf{r})|,t)$ are edge sensitive diffusion coefficients and enhancement operator respectively. The Perona-Malik equation is recovered at $q = 0$ and $e(u(\mathbf{r}),|\nabla u(\mathbf{r})|,t) = 0$. As in the original Perona-Malik equation, the hyper-diffusion coefficients $d_q(u(\mathbf{r}),|\nabla u(\mathbf{r})|,t)$ in Eq. (1) can be chosen in many different ways. For instance, one can set

$$d_q(u(\mathbf{r}),|\nabla u(\mathbf{r})|,t) = d_{q0} \exp\left[-\frac{|\nabla u|^2}{2\sigma_q^2} \right], \tag{2}$$

where the values of constants d_{q0} depend on the noise level, and σ_0 and σ_1 are chosen as the local statistical variance of u and ∇u

$$\sigma_q^2(\mathbf{r}) = \overline{|\nabla^q u - \overline{\nabla^q u}|^2} \quad (q = 0, 1). \tag{3}$$

The notation $\overline{Y(\mathbf{r})}$ above denotes the local average of $Y(\mathbf{r})$ centered at position $\mathbf{r}$. In this algorithm, the statistical measure based on the variance is important for discriminating image edges from noise. As such, one can bypass the image preprocessing, i.e., the convolution of the noise image with a test function or smooth mask.

In general, the nonlinear PDE operators described above serve as low-pass filters. PDE based nonlinear high-pass filters were introduced by Wei and Jia[31] in 2002. They constructed two weakly coupled

PDEs to act as a high-pass filter. Recently, this approach has been combined with Wei's earlier arbitrarily high order nonlinear PDE operator to give[23]

$$\partial_t \begin{pmatrix} u_m \\ v_n \end{pmatrix} = \begin{pmatrix} \sum_{j=0}^{m-1} \nabla \cdot d_{uj} \nabla \nabla^{2j} - \epsilon_{u_m} \ , \ \epsilon_{v_n} \\ \epsilon_{u_m} \ , \ \sum_{j=0}^{n-1} \nabla \cdot d_{vj} \nabla \nabla^{2j} - \epsilon_{v_n} \end{pmatrix} \begin{pmatrix} u_m \\ v_n \end{pmatrix},$$

where $\epsilon_{u_m} \equiv \epsilon_{u_m}(|\nabla u_m|)$ and $\epsilon_{u_n} \equiv \epsilon_{u_n}(|\nabla v_n|)$ are made edge sensitive. As low-pass filters, both $d_{uj} \equiv d_{uj}(|\nabla u_m|) \geq 0$ and $d_{vj} \equiv d_{vj}(|\nabla v_n|) \geq 0$ when j is even. Similarly, both $d_{uj}(|\nabla u_m|) \leq 0$ and $d_{vj}(|\nabla u_m|) \leq 0$ when j is odd. We can define a PDE transform as

$$w_{m,n}(\mathbf{r}, t) = u_m(\mathbf{r}, t) - v_n(\mathbf{r}, t) = H_{mn}(\mathbf{r}, t) X(\mathbf{r}), \tag{4}$$

where $H_{mn}(\mathbf{r}, t)$ can be regarded as a coupled nonlinear PDE operator. In order for Eq. (4) to work properly, we choose $|d_{vj}(|\nabla v_n|)| \gg |d_{uj}(|\nabla u_m|)|$. As shown in our earlier work, by increasing the order of the highest derivative, one can increase frequency localization and accuracy of the PDE transform for mode decomposition.[23] The frequency selection of $w_{m,n}(\mathbf{r}, t)$ also depends on the evolution time. High order PDEs are integrated by using the Fourier pseudospectral method.[23]

In the PDE transform, intrinsic mode functions w^k are systematically extracted from residues X^k, i.e.,

$$w_{mn}^k = H_{mn} X_{mn}^k, \quad \forall k = 1, 2, \cdots \tag{5}$$

where w_{mn}^k is the kth mode function. Here the residue function is given by

$$X_{mn}^k = X_{mn}^1 - \sum_{j=1}^{k-1} w_{mn}^j, \quad \forall k = 2, 3, \cdots . \tag{6}$$

where $X_{mn}^1 = X(\mathbf{r})$. Therefore, $X = \sum_{j=1}^{k-1} w_{mn}^j + X_{mn}^k$ is a perfect reconstruction of X in terms of all the mode functions and the last residue. The mode decomposition algorithm given in Eq. (5) is inherently nonlinear, even if a linear PDE operator might be used.

The PDE transform is applied to the image 1(a) to extract the three textures in Figures 1(b), 1(c) and 1(d). Note that only one texture is isolated at each time, which means the proposed PDE transform is able to perform a controlled or selective segmentation of textures. The PDEs of up to order 200 have been used for the selective texture segmentation. Numerically such high order linear PDE needs to be

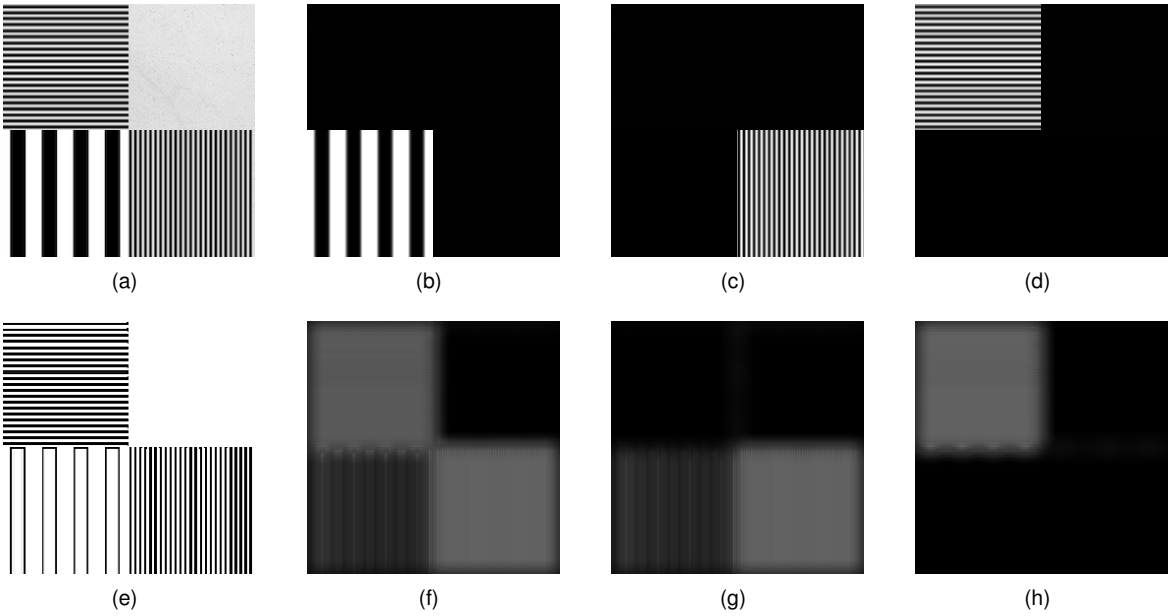

Figure 1: Extraction of various embedded textures using the PDE transform. Figure 1(a) shows the original image composed of various horizontal and vertical textures. Figures 1(b) through 1(d) show the three texture patterns extracted by applying the PDE transform, one at each time. Figure 1(e) shows the edge mode obtained by applying the PDE transform to Figure 1(a). Figure 1(f) shows the variance of the local variation of the image mode function 1(e). Figures 1(g) and 1(h) show the projection, or average, of the variance in Figure 1(f) along x- and y-direction respectively.

solved in the frequency domain.[23] Due to the ideal frequency localization, three textures are separated with clear boundary sharpness.

III Adaptive PDE transform algorithm

The separation of textures that are highly entangled in spatial locations, frequency ranges and gray scales becomes a challenge and conventional segmentation techniques are in general not applicable for such cases. For example, highly oscillatory textures can be separated from slowly varying background, but can not be separated from another texture with overlapping frequency distribution purely based on frequency fingerprints. To selectively distinguish such entangled textures of high frequency, one needs a mode decomposition algorithm that is able to be highly localized in frequency. Second order PDEs are poorly localized in the frequency domain.[23] Whereas, the PDE transform with high order PDEs provides desirable frequency localization.[23] However, the PDE transform by itself does not perform well for the separation of entangled textures. To this end, we introduce an adaptive PDE transform algorithm for selective texture extraction. The essence of the adaptive PDE algorithm lies in the realization that features of various textures are closely correlated with both the magnitude and smoothness of the gray scale values, or, equivalently, the local variation of the image mode functions. Similar ideas have been implemented in other methods such as total variation.[16]

Nonlinear PDEs have been widely applied to detect images with noises. However, despite of better image edge protection, the nonlinear anisotropic diffusion operator may still break down when the gradient generated by noise is comparable to image edges and features.[32] Application of a pre-convolution with a smoothing function to the image can practically alleviate the instability and reduce gray scale oscillation, but the image quality is often degraded. One alternative solution introduced by Wei[28] is to statistically discriminate noise from image edges by a measure based on the local statistical variance of the image or its gradient. Such a local statistical variance based edge-stopping algorithm was found to work very well for image restoration.

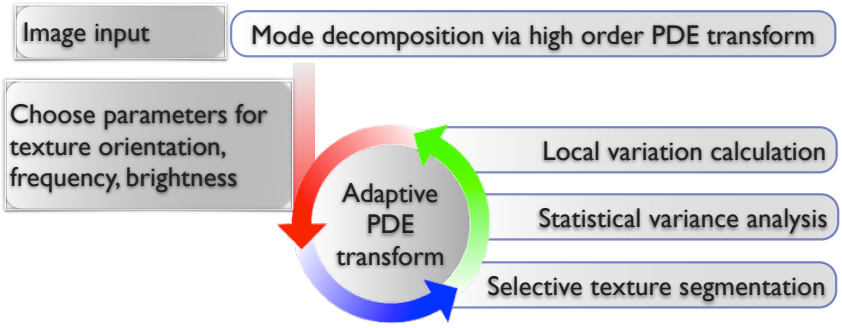

Figure 2: Algorithm of adaptive PDE transform for entangled texture separation.

Similar statistical analysis can be employed to perform selective texture extraction for images containing highly entangled and overlapping textures. In the present approach, we first compute the local variation of each pixel of the image mode functions obtained by the high order PDE transform. Unlike the total variation, the local variation is a still a function, of which the variance can be calculated

$$E(X(\mathbf{r})) = \overline{\left||\nabla X^k(\mathbf{r})| - \overline{|\nabla X^k(\mathbf{r})|}\right|^2}. \tag{7}$$

where $X^k(\mathbf{r})$ is the kth mode function obtained by the PDE transform (6) and $\left|\nabla X^k(\mathbf{r})\right|$ is evaluated locally over the neighbor pixels. Equation (7) yields a statistical analysis which is used for various texture separation and segmentation with appropriate threshold values. Various threshold values need to be chosen to select the range of the variance corresponding to the particular texture of interest. All the previously classified textures are registered for sequential/recursive texture extractions. A flowchart of the adaptive algorithm of PDE transform is shown in Figure 2.

Figure 1(e) shows the edge mode obtained by applying the PDE transform to Figure 1(a). Figure 1(f) shows the variance of the local variation of gray scale calculated using the adaptive PDE transform. Figures 1(g) and 1(h) show the projection, or average, of the variance in Figure 1(f) along x- and y-

direction respectively. By slicing out different domain of the variance in Figure 1(f), three different textures in Figures 1(b) through 1(d) are then perfectly separated from each other.

IV Applications

In this section, the adaptive PDE transform is applied to three different cases to illustrate its superior capability of selective texture separation. The three images feature different types of entangled textures. Figure 3(a) contains textures overlapping in the physical space with entangled frequency fingerprints. Figures 5(a) and 6(a) contain spatially segmented textures overlapping in the frequency domain. Figure 7 contains textures with overlapping textures highly entangled in both the frequency and spatial domains.

IV.A Text-image separation

The adaptive PDE transform method employing the variance of the local variation of the image mode functions is applied to several benchmark test cases. In particular, separation of text and texture can be regarded as a generalized type of texture analysis. In Figure 3, texts of various fonts are imprinted on the background image. Additional background watermark in Chinese is also presented in the image 3(a). The separation of English title from both background image and Chinese characters is a challenging task in terms of texture analysis because of the high degree of entanglement of very similar textures. Due to the font size difference in this application, high order PDE transform plays an extremely important role in differentiating modes with slightly different frequency characteristics. In Figure 3(b), the PDE transform successfully suppresses the low frequency parts and extracts the mode with frequency band mainly corresponding to texts. Such a procedure is similar to the edge detection in a general image processing. Statistical segmentation is then performed on the high frequency mode. A suitable threshold value is used to cut off the region with low variance and yields only the texts as shown in Figure 3(c).

(a) Original image. (b) Mode function. (c) Extracted texture.

Figure 3: Extraction and separation of texts, background watermark, and textures of image 3(a). Shown in the3(b) and 3(c) are the image mode function and extracted texture using the proposed adaptive PDE transform.

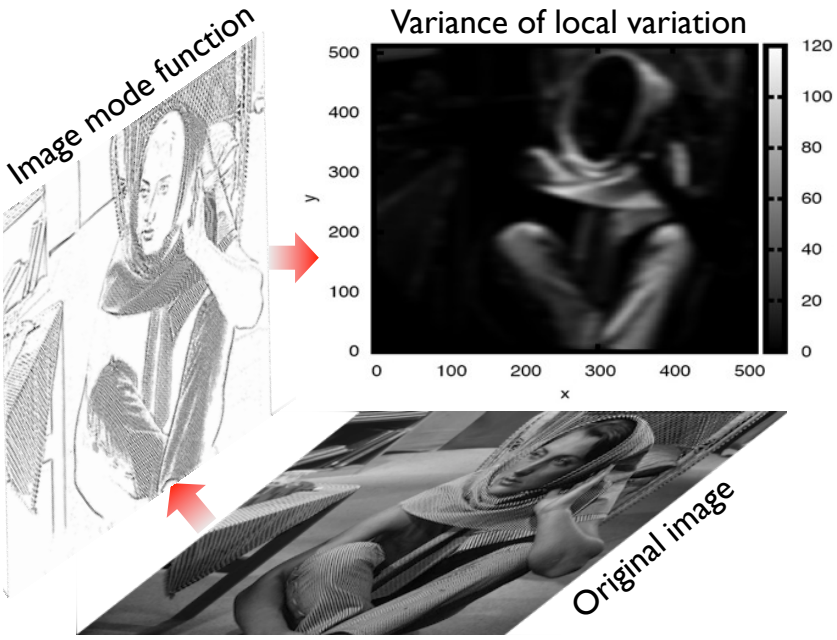

Figure 4: Adaptive PDE transform for selective texture extraction in the Barbara image. The variance of the local variation is shown in the top chart.

IV.B Selective texture extraction

The present algorithm of selective texture extraction is also tested on one of the most widely used images, the Barbara, in Figure 5. Barbara image is a benchmark test for edge detection and denoising. It contains fine details of different textures such as the table cloth, curtain behind Barbara, scarf and clothes on her. Distinctions between all these textures and the background is much larger than those among these textures, which leads to the difficulty of selective texture separation and segmentation. Due to the tiny difference between the frequency or spectrum features of different textures mentioned above, a highly frequency-selective separation method is required. However, the conventional Fourier method is not applicable for this case since the textures are entangled in the frequency domain. Moreover, conventional statistical segmentation approaches do not perform well for this case due to the gray scale entanglement. The present adaptive PDE transform method performs well for the selective texture extraction in the Barbara image. The total texture, or image edge, is extracted from the high frequency mode of the PDE transform as shown in Figure 5(b). The variance of the local variation is shown in Figure 4, which is calculated and employed for selective texture extraction and separation with appropriate thresholding values. The resulting textures are shown in the Figures 5(c) through 5(f) which correspond to those of clothes, curtain and table cloth, respectively. The four textures in the Figure 5 are superimposed on the original image for the purpose of a clearer visualization.

(a) Original image.

(b) Image mode function.

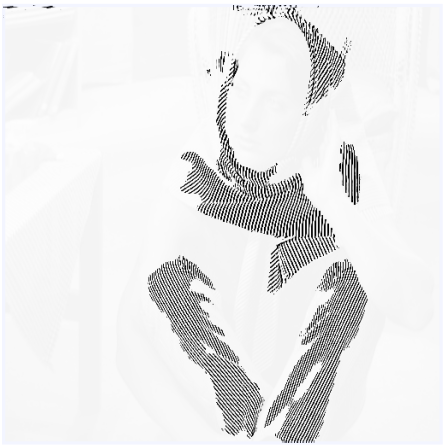

(c) Texture 1

(d) Texture 2

(e) Texture 3

(f) Texture 4

Figure 5: PDE transform is applied on image 5(a) to extract edges of all textures into 5(b). Adaptive PDE transform is then applied to extract different textures from 5(b). In 5(c) through 5(f), all the textures are superimposed on the original image for better viewing.

In Figure 6, the present adaptive PDE transform is applied to detect a sniper hidden in the forest (Figure 6(a)). The whole image is composed of highly entangled textures. The boundaries between these textures are very challenging to be identified appropriately. In our approach, variance of the local variation is calculated and used for texture separation as in the previous examples. By appropriate thresholding, the variance can be decomposed into three regions corresponding to those of the forest, the tree trunk, and the sniper. The resulting texture modes are shown in Figures 6(b) through 6(d).

(a) Original image.

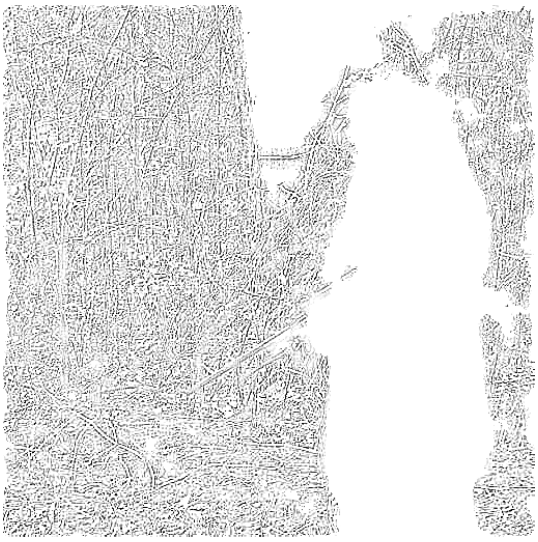

(b) Texture 1

(c) Texture 2

(d) Texture 3

Figure 6: Sniper detection by using adaptive PDE transform method. Textures 1, 2 and 3 are respectively from the forest, the tree trunk and the sniper.

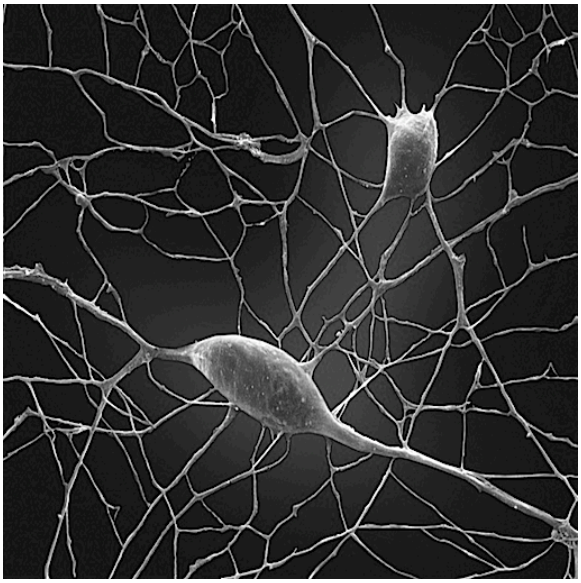

(a) Original neuron image.

(b) Class 1 of the selective neuron skeleton.

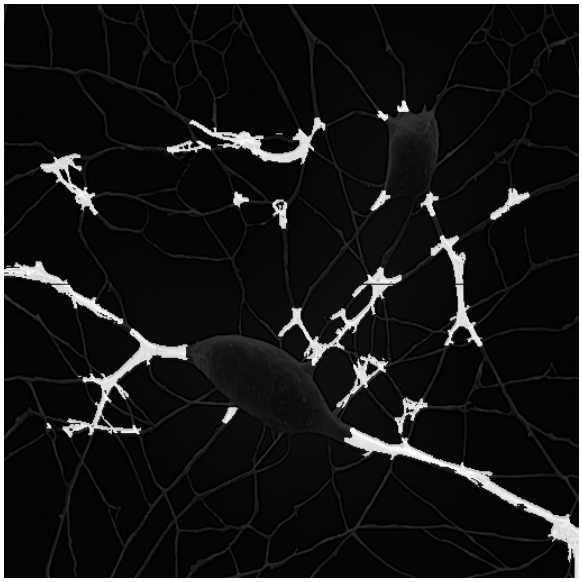

(c) Class 2 of the selective neuron skeleton.

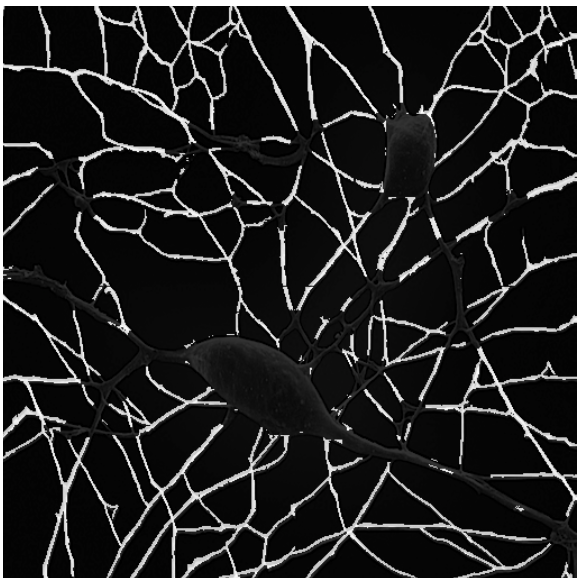

(d) Class 3 of the selective neuron skeleton.

Figure 7: Neuron image.

IV.C Natural neuron skeleton analysis

In the previous introduction to the adaptive PDE transform algorithm and applications, local variation is defined and calculated for the intensity of image mode functions to selectively extract textures beyond the total texture extraction. The selective texture extraction can be generalized to indicate any spatial parts of the image characterized with specific (and usually functionally important) spatial orientation and/or

Neuron skeleton class	Physical meaning	Percentage of the total neuron surface area
Class 1 shown in Figure 7(b)	Soma (neuron cell body)	22%
Class 2 shown in Figure 7(c)	Major (root of) dendrite	24%
Class 3 shown in Figure 7(d)	Fine (tips of) dendrite	54%

Table 1: Classification of natural neuron skeletons.

frequency oscillation, such as different parts in the neuron network, brain cells, and retina vasculatures. In Figure 7(a), the image of a typical neuron is shown. With advanced imaging techniques made available, research scientists have been able to obtain more and clearer 2D images and 3D data of various neuron cells and networks, whose study will be important for identifying the relation between phenotype and genotype pattens in physiology and molecular biology. Closely related to the advancement in the experimental imaging techniques, various improved computational image processing techniques have been proposed to better analyze neuron images. Neuron morphology study has become more and more important since the shape and branching of dendrites in neurons are closely related to the structure and functioning of the neuron network. Advancements in both experimental imaging techniques and computational image enhancements have led to better visualization and exploration of neuron morphology.[34,35,37–41] In the study of neuron morphology, image processing and segmentation of cultured neuron skeletons provides details of how neuron grow and branches. In this work, we apply the adaptive PDE transform to the study of "natural" neuron skeleton to segment and classify neuron skeletons into desirable classes according to the spatial extension and frequency oscillation of neuron dendrites, very much like the way of dividing a total image texture into several selective fine textures. Such separation and classification enable secondary processing and analysis of neuron morphology, such as the computation of surface areas (for 2D images) or volumes (for 3D data) for different classes of neuron skeletons. Specifically, we aim to separate different parts, or textures, such as soma, dendrites, axon, terminal or lobe, and numerous ramifications, from the neuron imaging as shown in Figures 7(b) through 7(d), where three classes of neuron parts are separated according to the spatial extension and frequency oscillation. Surface area of each class is listed in the Table 1. Ratios of these surface areas and many other geometric ratios of neuron morphology are related, on both molecular and cellular levels, to the many physiological diseases as well as the classification of neuron networks.

V Conclusion

Selective extraction and separation of image textures involving spatial entanglement, gray scale mixing, and high frequency overlapping are challenging tasks in image analysis. In this work, we introduce an appropriate adaptation to our earlier partial differential equation (PDE) transform[23] to construct an adap-

tive PDE transform algorithm. The adaptation is realized via a proper thresholding with the statistical variance of the local variation of image functional mode functions. The present PDE transform enables one to decompose and separate modes with entanglement in both spatial and frequency domains. The proposed method is applied to several challenging benchmark images. Textures of very similar features in the same image are successfully decomposed and separated using the present adaptive PDE transform method.

Acknowledgment

This work was supported in part by NSF grants CCF-0936830 and DMS-1043034; NIH grant GM-090208; MSU Competitive Discretionary Funding Program grant 91-4600.

References

[1] F. Zhang, X. Ye, and W. Liu, "Image decomposition and texture segmentation via sparse representation", *IEEE Signal Process Lett.*, vol. 15, pp. 641–644, 2008

[2] Y. Dong and J. Ma, "Wavelet-based image texture classification using local energy histograms", *IEEE Signal Process Lett.*, vol. 18, pp. 247-250, 2011

[3] K. I. Kim, S. H. Park, and H. J. Kim, "Kernel principal component analysis for texture classification", *IEEE Signal Process Lett.*, vol. 8, pp. 39–41, 2001

[4] R. M. Haralick, "Statistical and structural approaches to texture", *Proceedings of the IEEE*, vol. 67, pp. 786–804, 1979

[5] H. Wechsler, "Texture analysis – a survey", *Signal Process.*, vol. 2, pp. 271–282, 1980

[6] A. C. Bovik "Analysis of multichannel narrow-band filters for image texture segmentation", *IEEE Trans. Signal Process*, vol. 39, pp. 2025–2043, 1991

[7] J. Malik, S. Belongie, T. Leung, and J. Shi, "Contour and texture analysis for image segmentation", *Int. J. Comput. Vision*, vol. 43, pp. 7–27, 2001

[8] M. Elad, J. L. Starck, P. Querre, and D. L. Donoho, "Simultaneous cartoon and texture image inpainting using morphological component analysis (MCA)", *Appl. Comput. Harmon. Anal.*, vol. 19, pp. 340–358, 2005

[9] A. Khotanzad and J. Y. Chen, "Unsupervised segmentation of textured images by edge detection in multidimensional feature", *IEEE Trans. Pattern Anal. Mach. Intell.*, vol. 11, pp. 414–421, 1989

[10] S. Peleg, J. Naor, R. Hartley, and D. Avnir, "'Multiple resolution texture analysis and classification', *IEEE Trans. Pattern Anal. Mach. Intell.*, vol. 6, pp. 518–523, 1984

[11] J. Mao and A. K. Jain, "Texture classification and segmentation using multiresolution simultaneous autoregressive models", *Pattern Recognit.*, vol. 25, pp. 173–188, 1992

[12] G. R. Cross and A. K. Jain, "Markov random field texture models", *IEEE Trans. Pattern Anal. Mach. Intell.*, vol. 5, pp. 25–39, 1983

[13] D. Geman, S. Geman, C. Graffigne, and P. Dong, "Boundary detection by constrained optimization", *IEEE Trans. Pattern Anal. Mach. Intell.*, vol. 12, pp. 609–628, 1990

[14] A. Khotanzad and R. L. Kashyap, "Feature selection for texture recognition based on image synthesis", *IEEE Trans. Syst. Man Cybern.*, vol. 17, pp. 1087–1095, 1987

[15] A. P. Pentland, "Shading into texture", *Artif. Intell.*, vol. 29, pp. 147-170, 1986

[16] L. I. Rudin, S. J. Osher, and E. Fatemi, "Nonlinear Total Variation Based Noise Removal Algorithms", *Physica D*, vol. 60, pp. 259–268, 1992

[17] V. Caselles, J. M. Morel, G. Sapiro, and A. Tannenbaum, "Introduction to the special issue on partial differential equations and geometry-driven diffusion in image processing and analysis", *IEEE Trans. Image Process.* , vol. 7, pp. 269–273, 1998

[18] L. A. Vese and S. J. Osher, "Modeling textures with total variation minimization and oscillating patterns in image processing", *J. Sci. Comput.*, vol. 19, pp. 553–572, 2003

[19] F. Crosby and S. H. Kang, "Multiphase Segmentation for 3D Flash Lidar Images", *Journal of Pattern Recognition Research*, vol 6, pp. 193-200, 2011

[20] S. Krishnamachari and R. Chellappa, "Multiresolution Gauss-Markov random field models for texture segmentation", *IEEE Trans. Image Process.*, vol. 6, pp. 251–267, 1997

[21] Y. Wang, G. W. Wei, S. Y. Yang, "Iterative filtering decomposition based on local spectral evolution kernel", *J. Sci. Comput.*, in press. DOI: 10.1007/s10915-011-9496-0

[22] Y. Wang, G. W. Wei, and S. Y. Yang, "Mode decomposing evolution equations", *J. Sci. Comput.*, to be published. DOI: 10.1007/s10915-011-9509-z

[23] Y. Wang, G. W. Wei, and S. Y. Yang, “Partial differential equation transform: Variational formulation and Fourier analysis”, *Int. J. Numer. Methods Biomed. Eng.*, in press. DOI: 10.1002/cnm.1452

[24] Q. Zheng, S. Y. Yang, and G. W. Wei, “Biomolecular surface construction by PDE transform”, *Int. J. Numer. Methods Biomed. Eng*, in press. DOI: 10.1002/cnm.1469

[25] L. Hu, S. Y. Yang, Q. Zheng, and G. W. Wei, “PDE transform for hyperbolic conservation laws”, *J. Comput. Phys.*, 2011.

[26] A. P. Witkin, “Scale-space filtering”, in *Readings in computer vision: issues, problems, principles, and paradigms*, pp. 329–332, 1987

[27] P. Perona and J. Malik, “Scale-space and edge-detection using anisotropic diffusion”, *IEEE Trans. Pattern Anal. Mach. Intell.*, vol. 12, pp. 629–639, 1990

[28] G. W. Wei, “Generalized Perona-Malik equation for image restoration”, *IEEE Signal Process Lett.*, vol. 6, pp. 165–167, 1999

[29] Y. L. You and M. Kaveh, “Fourth-order partial differential equations for noise removal”, *IEEE Trans. Image Process.*, vol. 9, pp. 1723–1730, 2002

[30] M. Lysaker, A. Lundervold, and X. C. Tai, “Noise removal using fourth-order partial differential equation with application to medical magnetic resonance images in space and time”, *IEEE Trans. Image Process.*, vol. 12, pp. 1579–1590, 2003

[31] G. W. Wei and Y. Q. Jia, “Synchronization-based image edge detection”, *Europhys. Lett.*, vol. 59, pp. 814–819, 2002

[32] M. Nitzberg and T. Shiota, “Nonlinear image filtering with edge and corner enhancement”, *IEEE Trans. Pattern Anal. Mach. Intell.*, vol. 14, pp. 826, 1992

[33] M. Bertalmio, “Strong-continuation, contrast-invariant inpainting with a third-order optimal PDE”, *IEEE Trans. Image Process.*, vol. 15, pp. 1934–1938, 2006

[34] R. Yuste and T. Bonhoeffer, “Morphological changes in dendritic spines associated with long-term synaptic plasticity”, *Annu. Rev. Neurosci.*, vol. 24, pp. 1071–1089, 2001

[35] R. A. Graf and I. M. Cooke, “Outgrowth morphology and intracellular calcium of crustacean neurons displaying distinct morphologies in primary culture”, *J. Neurobiol.*, vol. 25, pp. 1558–1569, 1994

[36] M. Migliore, E. P. Cook, D. B. Jaffe, D. A. Turner, and D. Johnston, “Computer simulations of morphologically reconstructed CA3 hippocampal neurons”, *J. Neurophysiol.*, vol. 73, pp. 1157–1168, 1995

[37] J. C. Fiala, B. Allwardt, and K. M. Harris,“Dendritic spines do not split during hippocampal ltp or maturation”, *Nature Neurosci.*, vol. 5, pp. 297298, 2002

[38] R. F. Dacheux, M. F. Chimento, and F. R. Amthor,“Synaptic input to the on-off directionally selective ganglion cell in the rabbit retina”, *J. Comp. Neurol.*, vol. 456, pp. 267278, 2003

[39] P. J. Broser, R. Schulte, S. Lang, A. R. Fritjof, J. Waters, B. Sakmann, and G. Wittum, “Nonlinear anisotropic diffusion filtering of three-dimensional image data from two-photon microscopy”, *J. Biomed. Opt.*, vol. 9, pp. 1253-1264, 2004

[40] E. Jurrus, M. Hardy, T. Tasdizen, P. T. Fletcher, P. Koshevoy, C. B. Chien, W. Denk, and R. Whitaker, “Axon tracking in serial block-face scanning electron microscopy”, *Med. Image. Analys.*, vol. 13, pp. 180–188, 2009

[41] Y. Livneh and A. Mizrahi, “Long-term changes in the morphology and synaptic distributions of adult-born neurons”, *J. Comp. Neurol.*, vol. 519, pp. 2212–2224, 2011

[42] A. Haddad and Y. Meyer, “An improvement of Rudin-Osher-Fatemi model”, *Appl. Comput. Harmon. Anal.*, vol. 22, pp. 319–334, 2007

[43] J.B. Garnett, T.M. Le, Y. Meyer, and , L. A. Vese, “Image decompositions using bounded variation and generalized homogeneous Besov spaces”, *Appl. Comput. Harmon. Anal.*, vol. 23, pp. 25–56, 2007

[44] J. Gilles and Y. Meyer, “Properties of BV - G Structures plus Textures Decomposition Models. Application to Road Detection in Satellite Images”, *IEEE Trans. Image Process.*, vol. 19, pp. 2793-2800, 2010

[45] P. Maurel, J.F. Aujol, and G. Peyre, “Locally parallel texture modeling”, *SIAM J. Imag. Sci.*, vol. 4, pp. 413-447, 2011

[46] V. Duval, J.F. Aujol, and L.A. Vese, “Mathematical modeling of textures: application to color image decomposition with a projected gradient algorithm”, *J. Math. Imaging Vision*, vol. 37, pp. 232–248, 2010